Kai Li
Department of Civil Engineering,
Anhui Jianzhu University,
Hefei 230601, Anhui, China;
Department of Mechanical and
Aerospace Engineering,
University of California, San Diego,
La Jolla, CA 92093

Wanfang Wu
Department of Mechanical and
Aerospace Engineering,
University of California, San Diego,
La Jolla, CA 92093

Ziyang Jiang
Department of Mechanical and
Aerospace Engineering,
University of California, San Diego,
La Jolla, CA 92093

Shengqiang Cai[1]
Department of Mechanical and
Aerospace Engineering,
University of California, San Diego,
La Jolla, CA 92093
e-mail: shqcai@ucsd.edu

Voltage-Induced Wrinkling in a Constrained Annular Dielectric Elastomer Film

Wrinkles can be often observed in dielectric elastomer (DE) films when they are subjected to electrical voltage and mechanical forces. In the applications of DEs, wrinkle formation is often regarded as an indication of system failure. However, in some scenarios, wrinkling in DE does not necessarily result in material failure and can be even controllable. Although tremendous efforts have been made to analyze and calculate a variety of deformation modes in DE structures and devices, a model which is capable of analyzing wrinkling phenomena including the critical electromechanical conditions for the onset of wrinkles and wrinkle morphology in DE structures is currently unavailable. In this paper, we experimentally demonstrate controllable wrinkling in annular DE films with the central part being mechanically constrained. By changing the ratio between the inner radius and outer radius of the annular films, wrinkles with different wavelength can be induced in the films when externally applied voltage exceeds a critical value. To analyze wrinkling phenomena in DE films, we formulate a linear plate theory of DE films subjected to electromechanical loadings. Using the model, we successfully predict the wavelength of the voltage-induced wrinkles in annular DE films. The model developed in this paper can be used to design voltage-induced wrinkling in DE structures for different engineering applications. [DOI: 10.1115/1.4038427]

1 Introduction

A dielectric elastomer (DE) can deform when it is under the action of electrical field or mechanical forces. Because of the advantages of easy fabrication, low cost, excellent deformability, and electromechanical robustness, DEs have been recently intensively explored and developed to a variety of structures with diverse functions [1,2]. For instance, DE films with different shapes and sizes have been fabricated to harvest energy from different sources such as ocean wave [3], motions of human-beings, wind, and even combustion [4]. DEs have also been used as artificial muscles in designing walking robots [5], programmable grippers [6], camouflage devices [7], and antifouling systems [8]. In addition to those, transparent DE loudspeakers [9], planar DE rotary motors [10], and nonlinear DE strain gauges [11] have also been successfully made recently.

In most of the applications, large deformation in DEs can be ubiquitously observed. General three-dimensional (3D) models for the finite deformation of DEs under the actions of an arbitrary field of electrical potential and forces have been formulated by different researchers [12–18]. Numerous phenomena associated with the electromechanical coupling in DEs have been successfully analyzed using these developed models, such as the pull-in instability in a DE membrane sandwiched by two compliant electrodes [19–21], voltage-induced creasing and cratering instabilities in a constrained DE layer [22], giant deformation and shape bifurcation in DE balloons [23,24], and instabilities in layered soft dielectrics [25,26].

Because large deformation in a DE requires relatively large electric field, thin DE films are frequently adopted in most applications. As a consequence, multiple wrinkles can be often observed in the experiments in DE structures when they are subjected to electromechanical loading. Wrinkle formation has been often regarded as one of the failure mechanisms in DE devices [27–32]. In the last few years, it has been shown that in certain conditions, wrinkle formation in DE structures can be reversible and leads to no damage of the material [27,33–38]. Moreover, the wrinkles in DE structures may provide additional functions which cannot be easily obtained otherwise.

To predict the critical conditions of wrinkling in a DE film under different electromechanical loading, the film is usually assumed to be under plane stress condition. Because DE films are thin and can bear little compression, the external electromechanical loading which leads to the loss of tension at any point of the DE film is commonly adopted to represent the critical condition for the wrinkle formation [39–44] or failure of the structure. Reasonable agreements between the predictions and experimental measurements of the conditions for the onset of wrinkles in DE membranes have been obtained in several different studies [33,41,45,46].

Nevertheless, though the loss of tension can be used to estimate the critical conditions for the wrinkle formation in a DE film, analyses based on plane stress assumption cannot provide additional information about wrinkle morphology such as wavelength of wrinkles. Considering the recent interests in harnessing instabilities of soft active structures to achieve novel functions, a theoretical method which can accurately predict the critical conditions of wrinkling and the morphology of wrinkles in a DE film subjected to electromechanical loading is highly desired.

Most current electromechanical constitutive models of DE films are based on membrane assumption. Specifically, stress in a DE film is assumed to be uniform along its thickness direction, and its bending stiffness is completely ignored. Such assumptions greatly simplify the way of computing stress/stretch field and electrical field in DE structures under different loading conditions. The

[1]Corresponding author.
Contributed by the Applied Mechanics Division of ASME for publication in the Journal of Applied Mechanics. Manuscript received October 17, 2017; final manuscript received November 4, 2017; published online November 22, 2017. Editor: Yonggang Huang.

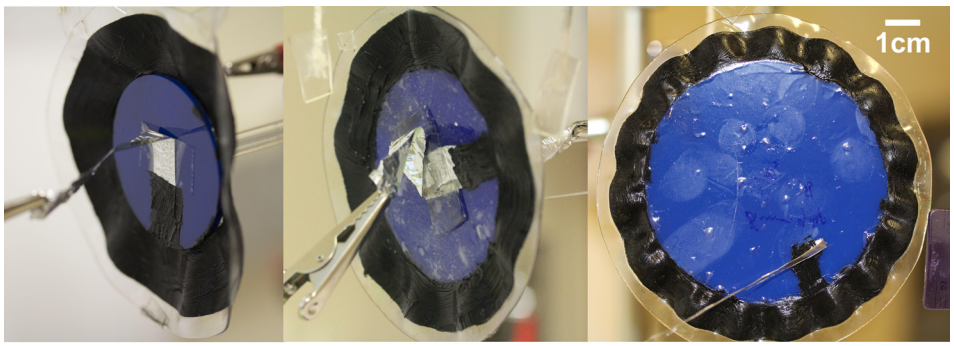

Fig. 1 Experimental photos of voltage-induced wrinkles in a constrained annular DE film with different ratios between the inner radius *A* and outer radius *B*: (*a*) *A*/*B* = 0.6, (*b*) *A*/*B* = 0.7, and (*c*) *A*/*B* = 0.8. The wavenumber of wrinkling mode increases with increasing radius ratio.

computational results based on the membrane assumption often agree well with experiments. However, the onset of wrinkles in a film is a result of competition between its bending energy and stretching energy. Therefore, taking account of the bending energy of a DE film becomes critical in analyzing the wrinkle formation and its morphology.

A general formulation of plate theory for DE films subjected to electromechanical loading is extremely challenging, which mainly stems from large deformation of the material, coupling between mechanics and electrical field, and complex geometries. To develop a model for predicting the critical condition of wrinkling instability, instead of establishing a general plate theory for DE thin films, we analyze the problem with a small three-dimensional displacement field associated with bending deformation superposed onto a finite two-dimensional deformation state of a DE film. Because the additional three-dimensional displacement field is small and we only focus on the bending of the DE film, we prescribe the form of additional displacement field by following Kirchhoff assumptions of linear plate theory.

Wrinkling in an annular membrane, caused by surface tension [47], inhomogeneous growth [48,49], and mechanical force [50,51], has been intensively studied in the past. As a demonstration of the application of our model, in this paper, we analyze the wrinkle formation in an annular DE film with internal constraint as shown in Fig. 1.

2 Experiment

In the experiment, we use laser cutter to cut a circular DE film (VHB 4905 purchased from 3M company (Maplewood, MN)) and paint carbon grease on both surfaces of the DE film as compliant electrode. To avoid electrical arcing across free edge of the film, we intentionally leave an annular gap near the edge of the film unpainted as shown in Fig. 1. We next glue a circular acrylate plate with different diameters on the center of the DE film to constrain its deformation. The adhesion between VHB film and the acrylate plate is strong enough, and no debonding and sliding have been observed in our experiments. Finally, we apply an electrical voltage across the thickness of the annular DE film with gradually increasing the magnitude. When the voltage is high enough, wrinkles can be clearly observed in the film. Depending on the size of the central rigid plate, wrinkles with different wavelength may appear as shown in Fig. 1. If the voltage in the experiments is not too high (e.g., below 10 kV), the formation and annihilation of wrinkles can repeat many times with the voltage being turned on and off.

3 Model and Formulation

3.1 A Constrained Annular DE Film Subjected to an Electrical Voltage. Figure 2 sketches an annular DE film with clamped inner boundary. In the undeformed state, the thickness of the film is denoted by H. The inner radius and outer radius of the annular plate are denoted by A and B, respectively. In the actuated state, a voltage Φ is applied between the two surfaces of the film. When the voltage is small, the DE film deforms axisymmetrically and maintains flat configuration (Fig. 2(*b*)). The hoop stress in the DE film is compressive, while the radial stress is always tensile. With increasing the voltage, the compressive hoop stress increases, and finally, wrinkles form in the DE film as shown in

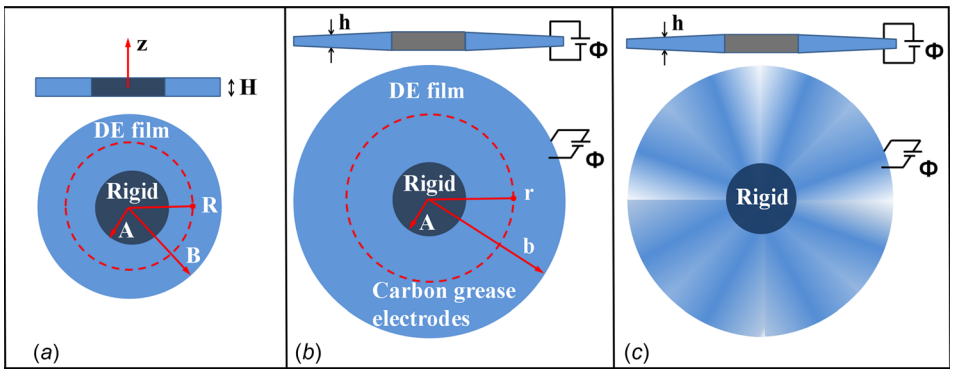

Fig. 2 Schematics of an annular DE film constrained by an inner circular rigid plate. The inner radius and outer radius of the annular DE film without deformation are denoted by *A* and *B*, respectively. In the experiment, an electrical voltage Φ is applied across the thickness of the DE film. Three different states of the annular DE film are sketched: (*a*) undeformed state, (*b*) deformed state without wrinkles, and (*c*) wrinkled state.

Figs. 1 and 2(*c*). In the following, we first analyze the deformation of DE film without wrinkles.

In the reference state, we label each material particle by its radial coordinate R in the interval (A, B). In a deformed state, the material particle R takes the position of coordinate $r(R)$. The function $r(R)$ describes the deformed state of the DE film. The radial stretch and the hoop stretch can be calculated as

$$\lambda_r = \frac{dr}{dR} \tag{1}$$

$$\lambda_\theta = \frac{r}{R} \tag{2}$$

The DE is assumed to be incompressible, so that the stretch in thickness direction is $\lambda_z = 1/\lambda_r\lambda_\theta$.

The electrical field E in the DE film is along the normal direction of the film and relates to the voltage Φ as

$$E = \frac{\Phi}{h} \tag{3}$$

where h is the thickness of the film in the deformed state, so $h = H\lambda_z$.

The equation of force balance in the annular DE film is given by

$$\frac{d}{dR}\left(\frac{\sigma_{rr}}{\lambda_r}\right) - \frac{1}{R}\left(\frac{\sigma_{\theta\theta}}{\lambda_\theta} - \frac{\sigma_{rr}}{\lambda_r}\right) = 0 \tag{4}$$

In this paper, we adopt ideal dielectric elastomer model, which assumes electrical permittivity ε is a constant and unaffected by the deformation and electrical field [16]. Meanwhile, neo-Hookean model is adopted here to describe the hyperelasticity of the material. As a consequence, we have the following constitutive equation:

$$\sigma_{rr} = \mu(\lambda_r^2 - \lambda_r^{-2}\lambda_\theta^{-2}) - \varepsilon E^2 \tag{5}$$

$$\sigma_{\theta\theta} = \mu(\lambda_\theta^2 - \lambda_r^{-2}\lambda_\theta^{-2}) - \varepsilon E^2 \tag{6}$$

where the first term in Eqs. (5) and (6) originates from the elasticity of the elastomer, and the second term is known as Maxwell stress.

From the equilibrium equation (4), we can obtain the first derivative of $\lambda_r(R)$

$$\frac{d\lambda_r}{dR} = \frac{\dfrac{\sigma_{\theta\theta}}{\lambda_\theta} - \dfrac{\sigma_{rr}}{\lambda_r} + (\lambda_\theta - \lambda_r)\dfrac{\partial}{\partial\lambda_\theta}\left(\dfrac{\sigma_{rr}}{\lambda_r}\right)}{R\dfrac{\partial}{\partial\lambda_r}\left(\dfrac{\sigma_{rr}}{\lambda_r}\right)} \tag{7}$$

First derivative of $\lambda_\theta(R)$ in Eq. (2) gives that

$$\frac{d\lambda_\theta}{dR} = \frac{\lambda_r - \lambda_\theta}{R} \tag{8}$$

The ordinary differential equations (ODEs) of Eqs. (7) and (8) can be solved numerically with the following two boundary conditions:

$$r(A) = A \tag{9}$$

$$\sigma_{rr}(B) = 0 \tag{10}$$

3.2 Linear Stability Analysis of Voltage-Induced Wrinkles in a DE Film. As discussed earlier, voltage-induced compressive hoop stress in the annular DE film may result in wrinkling. To investigate the formation and morphology of wrinkles, we first formulate a linear plate theory for a DE film under electromechanical loading.

To derive the governing equations for the deflection of a DE film, we first need to obtain the relationship between the stress and deflection of the film subjected to electromechanical loadings. For the purpose of clarity and simplicity, we first derive the stress–deflection relationship of a DE film in a Cartesian coordinate, and then, we transfer the results to a polar coordinate.

We consider an element of a DE film subjected to a homogeneous electrical field along the thickness direction. The deformation gradient of the film from initial undeformed state denoted by $\mathbf{B}_i$ to a flat state denoted by $\mathbf{B}_0$ is given by

$$\mathbf{F}_0 = \begin{bmatrix} \lambda_x & 0 & 0 \\ 0 & \lambda_y & 0 \\ 0 & 0 & \lambda_z \end{bmatrix} \tag{11}$$

where λ_x, λ_y, and λ_z are the principle stretches in three orthogonal directions x, y, and z, where x and y are two perpendicular directions in the plane of the film, and z is the direction perpendicular to the film.

Next, we assume the displacement field associated with wrinkling deformation can be represented by u, v, and w in the three orthogonal directions x, y, and z. The deformation gradient from the predeformed state $\mathbf{B}_0$ to wrinkled state $\mathbf{B}_1$ can be given by

$$\mathbf{F}_1 = \begin{bmatrix} 1 + \dfrac{\partial u}{\partial x} & \dfrac{\partial u}{\partial y} & \dfrac{\partial u}{\partial z} \\ \dfrac{\partial v}{\partial x} & 1 + \dfrac{\partial v}{\partial y} & \dfrac{\partial v}{\partial z} \\ \dfrac{\partial w}{\partial x} & \dfrac{\partial w}{\partial y} & 1 + \dfrac{\partial w}{\partial z} \end{bmatrix} \tag{12}$$

Therefore, the deformation gradient from initial state $\mathbf{B}_i$ to wrinkled state $\mathbf{B}_1$ can be calculated as

$$\mathbf{F} = \mathbf{F}_1 \cdot \mathbf{F}_0 = \begin{bmatrix} \lambda_x\left(1 + \dfrac{\partial u}{\partial x}\right) & \lambda_y\dfrac{\partial u}{\partial y} & \lambda_z\dfrac{\partial u}{\partial z} \\ \lambda_x\dfrac{\partial v}{\partial x} & \lambda_y\left(1 + \dfrac{\partial v}{\partial y}\right) & \lambda_z\dfrac{\partial v}{\partial z} \\ \lambda_x\dfrac{\partial w}{\partial x} & \lambda_y\dfrac{\partial w}{\partial y} & \lambda_z\left(1 + \dfrac{\partial w}{\partial z}\right) \end{bmatrix} \tag{13}$$

The corresponding left Cauchy-Green strain tensor is

$$\mathbf{B} = \mathbf{F} \cdot \mathbf{F}^{\mathrm{T}} = \begin{bmatrix} \lambda_x^2\left(1 + 2\dfrac{\partial u}{\partial x}\right) & \lambda_x^2\dfrac{\partial v}{\partial x} + \lambda_y^2\dfrac{\partial u}{\partial y} & \lambda_x^2\dfrac{\partial w}{\partial x} + \lambda_z^2\dfrac{\partial u}{\partial z} \\ \lambda_x^2\dfrac{\partial v}{\partial x} + \lambda_y^2\dfrac{\partial u}{\partial y} & \lambda_y^2\left(1 + 2\dfrac{\partial v}{\partial y}\right) & \lambda_y^2\dfrac{\partial w}{\partial y} + \lambda_z^2\dfrac{\partial v}{\partial z} \\ \lambda_x^2\dfrac{\partial w}{\partial x} + \lambda_z^2\dfrac{\partial u}{\partial z} & \lambda_y^2\dfrac{\partial w}{\partial y} + \lambda_z^2\dfrac{\partial v}{\partial z} & \lambda_z^2\left(1 + 2\dfrac{\partial w}{\partial z}\right) \end{bmatrix} \tag{14}$$

Based on ideal dielectric elastomer model, Cauchy stress in a DE film can be decomposed into elastic part and Maxwell stress, namely,

$$\boldsymbol{\sigma} = \boldsymbol{\sigma}_{\mathrm{ela}} + \boldsymbol{\sigma}_{\mathrm{m}} \tag{15}$$

where Maxwell stress is a tensor and can be represented by

$$\boldsymbol{\sigma}_{\mathrm{m}} = \begin{bmatrix} -\frac{1}{2}\varepsilon E^2 & 0 & 0 \\ 0 & -\frac{1}{2}\varepsilon E^2 & 0 \\ 0 & 0 & \frac{1}{2}\varepsilon E^2 \end{bmatrix} \tag{16}$$

and elastic stress $\boldsymbol{\sigma}_{\mathrm{ela}}$ is given by

$$\boldsymbol{\sigma}_{\mathrm{ela}} = \mathbf{F}\frac{\partial W_{\mathrm{stretch}}}{\partial \mathbf{F}} - p\mathbf{I} \tag{17}$$

where W_{stretch} is the strain energy density of the elastomer, and p is the hydrostatic pressure for the incompressibility of the elastomer. We adopt neo-Hookean model in the current paper, so Eq. (17) can be written explicitly as

$$\boldsymbol{\sigma}_{\mathrm{ela}} = \mu\mathbf{B} - p\mathbf{I} \tag{18}$$

Substituting Eqs. (16) and (18) into Eq. (15) leads to

$$\boldsymbol{\sigma} = \begin{bmatrix} -p - \frac{\varepsilon E^2}{2} + \mu\lambda_x^2\left(1 + 2\frac{\partial u}{\partial x}\right) & \mu\left(\lambda_x^2\frac{\partial v}{\partial x} + \lambda_y^2\frac{\partial u}{\partial y}\right) & \mu\left(\lambda_x^2\frac{\partial w}{\partial x} + \lambda_z^2\frac{\partial u}{\partial z}\right) \\ \mu\left(\lambda_x^2\frac{\partial v}{\partial x} + \lambda_y^2\frac{\partial u}{\partial y}\right) & -p - \frac{\varepsilon E^2}{2} + \mu\lambda_y^2\left(1 + 2\frac{\partial v}{\partial y}\right) & \mu\left(\lambda_y^2\frac{\partial w}{\partial y} + \lambda_z^2\frac{\partial v}{\partial z}\right) \\ \mu\left(\lambda_x^2\frac{\partial w}{\partial x} + \lambda_z^2\frac{\partial u}{\partial z}\right) & \mu\left(\lambda_y^2\frac{\partial w}{\partial y} + \lambda_z^2\frac{\partial v}{\partial z}\right) & -p + \frac{\varepsilon E^2}{2} + \mu\lambda_z^2\left(1 + 2\frac{\partial w}{\partial z}\right) \end{bmatrix} \tag{19}$$

We can further rewrite Eq. (19) as

$$\frac{\partial u}{\partial x} = \frac{2\sigma_{xx} + 2p + \varepsilon E^2}{4\mu\lambda_x^2} - \frac{1}{2} \tag{20a}$$

$$\frac{\partial v}{\partial y} = \frac{2\sigma_{yy} + 2p + \varepsilon E^2}{4\mu\lambda_y^2} - \frac{1}{2} \tag{20b}$$

$$\frac{\partial w}{\partial z} = \frac{2\sigma_{zz} + 2p - \varepsilon E^2}{4\mu\lambda_z^2} - \frac{1}{2} \tag{20c}$$

$$\lambda_x^2\frac{\partial v}{\partial x} + \lambda_y^2\frac{\partial u}{\partial y} = \frac{\sigma_{xy}}{\mu} \tag{20d}$$

$$\lambda_x^2\frac{\partial w}{\partial x} + \lambda_z^2\frac{\partial u}{\partial z} = \frac{\sigma_{xz}}{\mu} \tag{20e}$$

$$\lambda_y^2\frac{\partial w}{\partial y} + \lambda_z^2\frac{\partial v}{\partial z} = \frac{\sigma_{yz}}{\mu} \tag{20f}$$

The incompressibility condition of the DE film requires that

$$\frac{\partial u}{\partial x} + \frac{\partial v}{\partial y} + \frac{\partial w}{\partial z} = 0 \tag{21}$$

A combination of Eqs. (20*a*)–(20*c*) and Eq. (21) gives that

$$p = \frac{3\mu\lambda_x^2\lambda_y^2 - \lambda_y^2\sigma_{xx} - \lambda_x^2\sigma_{yy} - \lambda_x^4\lambda_y^4\sigma_{zz} - \lambda_x^4\lambda_y^4\varepsilon E^2}{\lambda_x^2 + \lambda_y^2 + \lambda_x^4\lambda_y^4} - \frac{\varepsilon E^2}{2} \tag{22}$$

Substituting Eq. (22) into Eqs. (20*a*)–(20*f*), we can further obtain

$$\frac{\partial u}{\partial x} = \frac{3\mu\lambda_x^2\lambda_y^2 - \lambda_y^2\sigma_{xx} - \lambda_x^2\sigma_{yy} - \lambda_x^4\lambda_y^4\sigma_{zz} - \lambda_x^4\lambda_y^4\varepsilon E^2}{2\mu\lambda_x^2\left(\lambda_x^2 + \lambda_y^2 + \lambda_x^4\lambda_y^4\right)} - \frac{1}{2} \tag{23a}$$

$$\frac{\partial v}{\partial y} = \frac{3\mu\lambda_x^2\lambda_y^2 - \lambda_x^2\sigma_{yy} - \lambda_y^2\sigma_{xx} - \lambda_x^4\lambda_y^4\sigma_{zz} - \lambda_x^4\lambda_y^4\varepsilon E^2}{2\mu\lambda_y^2\left(\lambda_x^2 + \lambda_y^2 + \lambda_x^4\lambda_y^4\right)} - \frac{1}{2} \tag{23b}$$

$$\frac{\partial w}{\partial z} = \frac{3\mu\lambda_x^4\lambda_y^4 - \lambda_x^2\lambda_y^4\sigma_{xx} - \lambda_x^4\lambda_y^2\sigma_{yy} - \lambda_x^2\lambda_y^2\left(\lambda_x^2 + \lambda_y^2\right)\sigma_{zz} - \lambda_x^6\lambda_y^6\varepsilon E^2}{2\mu\left(\lambda_x^2 + \lambda_y^2 + \lambda_x^4\lambda_y^4\right)} - \frac{\lambda_x^2\lambda_y^2\varepsilon E^2}{2\mu} - \frac{1}{2} \tag{23c}$$

$$\lambda_x^2\frac{\partial v}{\partial x} + \lambda_y^2\frac{\partial u}{\partial y} = \frac{\sigma_{xy}}{\mu} \tag{23d}$$

$$\lambda_x^2\frac{\partial w}{\partial x} + \lambda_z^2\frac{\partial u}{\partial z} = \frac{\sigma_{xz}}{\mu} \tag{23e}$$

$$\lambda_y^2\frac{\partial w}{\partial y} + \lambda_z^2\frac{\partial v}{\partial z} = \frac{\sigma_{yz}}{\mu} \tag{23f}$$

A combination of Eqs. (23*a*)–(23*f*) and force balance equations gives a complete set of governing equations for both additional displacement field and stress field in a DE. However, without further simplifications, these equations are very difficult to solve. As

discussed previously, in this paper, we only focus on additional bending deformation in a DE film, so we will follow Kirchhoff's hypotheses [52] to further simplify the problem. Kirchhoff's hypotheses developed for linear plate theory state that the straight lines, initially normal to the middle plane of a plate before bending, remain straight and normal to the middle surface during bending, and the length of such plate elements does not change. Mathematically, we have the following equations:

$$\frac{\partial w}{\partial z} = 0 \tag{24a}$$

$$\frac{\partial w}{\partial x} + \frac{\partial u}{\partial z} = 0 \tag{24b}$$

$$\frac{\partial w}{\partial y} + \frac{\partial v}{\partial z} = 0 \tag{24c}$$

The three new equations ((24*a*)–(24*c*)) originating from Kirchhoff's hypotheses make the problem overdetermined. Therefore, it is necessary to drop three equations. Following conventional linear plate theory [52], Eqs. (23*c*), (23*e*), and (23*f*) are discarded. Moreover, the stress normal to the middle plane of the plate is assumed to be negligible compared with other stress components, i.e., $\sigma_{zz} = 0$. Finally, the nonzero stress components in the DE film can be expressed as

$$\begin{Bmatrix} \sigma_{xx} \\ \sigma_{yy} \\ \sigma_{xy} \end{Bmatrix} = \begin{Bmatrix} \mu\left(\lambda_x^2 - \lambda_x^{-2}\lambda_y^{-2}\right) - \varepsilon E^2 \\ \mu\left(\lambda_y^2 - \lambda_x^{-2}\lambda_y^{-2}\right) - \varepsilon E^2 \\ 0 \end{Bmatrix} + \begin{Bmatrix} 2\mu\left(\lambda_x^{-2}\lambda_y^{-2} + \lambda_x^2\right)\dfrac{\partial u}{\partial x} + 2\mu\lambda_x^{-2}\lambda_y^{-2}\dfrac{\partial v}{\partial y} \\ 2\mu\left(\lambda_x^{-2}\lambda_y^{-2} + \lambda_y^2\right)\dfrac{\partial v}{\partial y} + 2\mu\lambda_x^{-2}\lambda_y^{-2}\dfrac{\partial u}{\partial x} \\ \mu\left(\lambda_x^2\dfrac{\partial v}{\partial x} + \lambda_y^2\dfrac{\partial u}{\partial y}\right) \end{Bmatrix} \tag{25}$$

Integrating Eqs. (24*a*)–(24*c*), we can obtain the displacement of a material point in the DE film with distance z from the middle plane

$$\begin{Bmatrix} u_x^z \\ u_y^z \end{Bmatrix} = \begin{Bmatrix} -z\dfrac{\partial w}{\partial x} \\ -z\dfrac{\partial w}{\partial y} \end{Bmatrix} \tag{26}$$

where $w = w(x, y)$ is independent on z and denotes the deflection of the DE film.

Substituting Eq. (26) into Eq. (25), we can further obtain the stress components of a material point in the DE film with distance z from the middle plane

$$\begin{Bmatrix} \sigma_{xx}^z \\ \sigma_{yy}^z \\ \sigma_{xy}^z \end{Bmatrix} = \begin{Bmatrix} \mu\left(\lambda_x^2 - \lambda_x^{-2}\lambda_y^{-2}\right) - \varepsilon E^2 \\ \mu\left(\lambda_y^2 - \lambda_x^{-2}\lambda_y^{-2}\right) - \varepsilon E^2 \\ 0 \end{Bmatrix} - z\begin{bmatrix} C_{11} & C_{12} & 0 \\ C_{21} & C_{22} & 0 \\ 0 & 0 & 2C_{66} \end{bmatrix} \begin{Bmatrix} \dfrac{\partial^2 w}{\partial x^2} \\ \dfrac{\partial^2 w}{\partial y^2} \\ \dfrac{\partial^2 w}{\partial x \partial y} \end{Bmatrix} \tag{27}$$

where $C_{11} = 2\mu(\lambda_x^{-2}\lambda_y^{-2} + \lambda_x^2)$, $C_{22} = 2\mu(\lambda_x^{-2}\lambda_y^{-2} + \lambda_y^2)$, $C_{12} = C_{21} = 2\mu\lambda_x^{-2}\lambda_y^{-2}$, and $2C_{66} = \mu(\lambda_x^2 + \lambda_y^2)$.

In our model, we assume that the thickness of the DE film is small and the electrical field does not vary along the thickness direction. Then, the bending moments M_{xx}, M_{yy}, and twisting moment M_{xy} can be integrated as

$$\begin{Bmatrix} M_{xx} \\ M_{yy} \\ M_{xy} \end{Bmatrix} = \int_{-h/2}^{h/2} \begin{Bmatrix} \sigma_{xx}^z \\ \sigma_{yy}^z \\ \sigma_{xy}^z \end{Bmatrix} z dz = -\frac{H^3}{12\lambda_x^3\lambda_y^3}\begin{bmatrix} C_{11} & C_{12} & 0 \\ C_{21} & C_{22} & 0 \\ 0 & 0 & 2C_{66} \end{bmatrix} \begin{Bmatrix} \dfrac{\partial^2 w}{\partial x^2} \\ \dfrac{\partial^2 w}{\partial y^2} \\ \dfrac{\partial^2 w}{\partial x \partial y} \end{Bmatrix} \tag{28}$$

In a polar coordinate, the bending moments and twisting moment can be similarly written as

$$\begin{Bmatrix} M_{rr} \\ M_{\theta\theta} \\ M_{r\theta} \end{Bmatrix} = -\frac{H^3}{12\lambda_r^3\lambda_\theta^3}\begin{bmatrix} C_{rr} & C_{r\theta} & 0 \\ C_{\theta r} & C_{\theta\theta} & 0 \\ 0 & 0 & 2C_{ss} \end{bmatrix} \begin{Bmatrix} \dfrac{\partial^2 w}{\partial r^2} \\ \dfrac{1}{r}\dfrac{\partial w}{\partial r} + \dfrac{1}{r^2}\dfrac{\partial^2 w}{\partial \theta^2} \\ \dfrac{1}{r}\dfrac{\partial^2 w}{\partial r \partial \theta} - \dfrac{1}{r^2}\dfrac{\partial w}{\partial \theta} \end{Bmatrix} \tag{29}$$

where $C_{rr} = 2\mu(\lambda_r^{-2}\lambda_\theta^{-2} + \lambda_r^2)$, $C_{\theta\theta} = 2\mu(\lambda_r^{-2}\lambda_\theta^{-2} + \lambda_\theta^2)$, $C_{r\theta} = C_{\theta r} = 2\mu\lambda_r^{-2}\lambda_\theta^{-2}$, and $2C_{ss} = \mu(\lambda_r^2 + \lambda_\theta^2)$. Therefore, in a polar coordinate, we have

$$M_{rr} = -\left[D_{rr}\frac{\partial^2 w}{\partial r^2} + D_{r\theta}\left(\frac{1}{r}\frac{\partial w}{\partial r} + \frac{1}{r^2}\frac{\partial^2 w}{\partial \theta^2}\right)\right] \tag{30a}$$

$$M_{\theta\theta} = -\left[D_{\theta\theta}\left(\frac{1}{r}\frac{\partial w}{\partial r} + \frac{1}{r^2}\frac{\partial^2 w}{\partial \theta^2}\right) + D_{\theta r}\frac{\partial^2 w}{\partial r^2}\right] \tag{30b}$$

$$M_{r\theta} = M_{\theta r} = -2D_{ss}\left(\frac{1}{r}\frac{\partial^2 w}{\partial r \partial \theta} - \frac{1}{r^2}\frac{\partial w}{\partial \theta}\right) \tag{30c}$$

where $D_{rr} = \mu H^3(\lambda_r^{-5}\lambda_\theta^{-5} + \lambda_r^{-1}\lambda_\theta^{-3})/6$, $D_{\theta\theta} = \mu H^3(\lambda_r^{-5}\lambda_\theta^{-5} + \lambda_r^{-3}\lambda_\theta^{-1})/6$, $D_{r\theta} = D_{\theta r} = \mu H^3\lambda_r^{-5}\lambda_\theta^{-5}/6$, and $D_{ss} = \mu H^3(\lambda_r^{-1}\lambda_\theta^{-3} + \lambda_r^{-3}\lambda_\theta^{-1})/24$.

In the normal direction, force balance condition requires that

$$\frac{\partial^2 M_{rr}}{\partial r^2} + \frac{2}{r}\frac{\partial M_{rr}}{\partial r} + \frac{2}{r}\frac{\partial^2 M_{r\theta}}{\partial r \partial \theta} + \frac{2}{r^2}\frac{\partial M_{r\theta}}{\partial \theta} - \frac{1}{r}\frac{\partial M_{\theta\theta}}{\partial r} + \frac{1}{r^2}\frac{\partial^2 M_{\theta\theta}}{\partial \theta^2} + N_{rr}\frac{\partial^2 w}{\partial r^2} + 2N_{r\theta}\left(\frac{1}{r}\frac{\partial^2 w}{\partial r \partial \theta} - \frac{1}{r^2}\frac{\partial w}{\partial \theta}\right) + N_{\theta\theta}\left(\frac{1}{r}\frac{\partial w}{\partial r} + \frac{1}{r^2}\frac{\partial^2 w}{\partial \theta^2}\right) = 0 \tag{31}$$

where $N_{rr} = \sigma_{rr}h$, $N_{\theta\theta} = \sigma_{\theta\theta}h$, and $N_{r\theta} = \sigma_{r\theta}h$ are the membrane forces.

On the inner circular boundary, the DE film is clamped, namely,

$$w = 0 \tag{32}$$

$$\frac{\partial w}{\partial r} = 0 \tag{33}$$

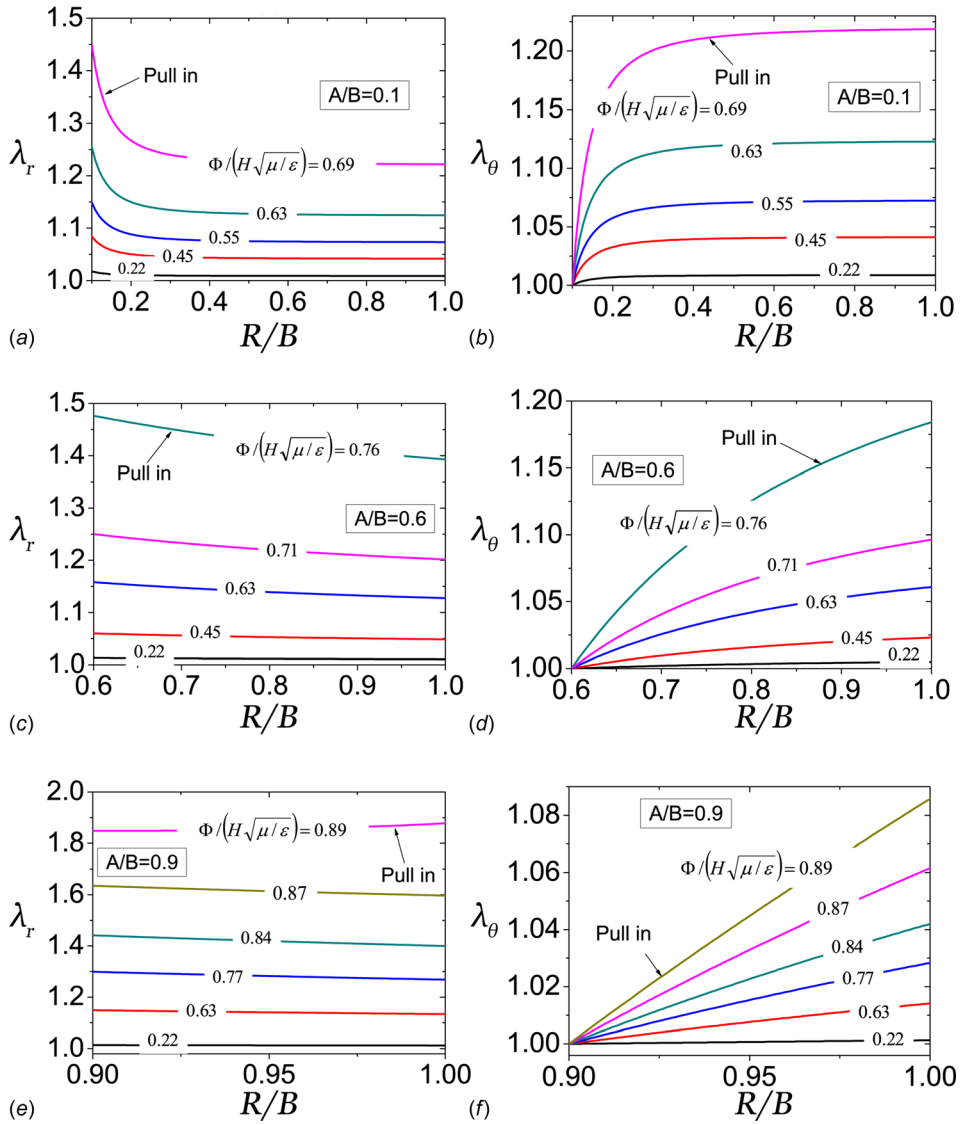

Fig. 3 Distributions of radial stretch and hoop stretch in a constrained annular DE film for several different voltages and ratios between its inner radius *A* and outer radius *B*: (*a*) and (*b*) *A*/*B* = 0.1, (*c*) and (*d*) *A*/*B* = 0.6, and (*e*) and (*f*) *A*/*B* = 0.9. The highest voltages in the figures correspond to the critical voltage of inducing pull-in instability in the DE film.

On the outer circular boundary, the bending moment is zero and vertical shear force is zero, namely,

$$M_{rr} = 0 \tag{34}$$

$$\frac{\partial M_{rr}}{\partial r} + \frac{2}{r}\frac{\partial M_{r\theta}}{\partial \theta} + \frac{M_{rr} - M_{\theta\theta}}{r} = 0 \tag{35}$$

A combination of Eqs. (30*a*)–(30*c*) and (31) with boundary conditions (Eqs. (32)–(35)) sets an eigenvalue problem. We assume the deflection of the DE film follows:

$$w = f(\bar{r})\cos(k\theta) \tag{36}$$

where $\bar{r} = r/B$, $f(\bar{r})$ is a single variable function, and k is wavenumber of wrinkle.

Inserting Eq. (36) into Eqs. (30) and (31), we get the following homogeneous ODE:

$$\begin{aligned}
&\left(\frac{d^4 f}{d\bar{r}^4} + \frac{2}{\bar{r}}\frac{d^3 f}{d\bar{r}^3}\right)\bar{D}_{rr} + 2\left(\frac{d^3 f}{d\bar{r}^3} + \frac{1}{\bar{r}}\frac{d^2 f}{d\bar{r}^2}\right)\frac{d\bar{D}_{rr}}{d\bar{r}} + \frac{d^2 f}{d\bar{r}^2}\frac{d^2 \bar{D}_{rr}}{d\bar{r}^2} \\
&+ \frac{1}{\bar{r}^2}\left(\frac{1}{\bar{r}}\frac{df}{d\bar{r}} - \frac{d^2 f}{d\bar{r}^2} + \frac{k^2 - 2}{\bar{r}^2}k^2 f\right)\bar{D}_{\theta\theta} - \frac{1}{\bar{r}^2}\left(\frac{df}{d\bar{r}} - \frac{k^2 f}{\bar{r}}\right)\frac{d\bar{D}_{\theta\theta}}{d\bar{r}} \\
&+ \frac{2k^2}{\bar{r}^2}\left(-\frac{f}{\bar{r}^2} + \frac{1}{\bar{r}}\frac{df}{d\bar{r}} - \frac{d^2 f}{d\bar{r}^2}\right)\bar{D}_{r\theta} + \frac{2k^2}{\bar{r}^2}\left(\frac{f}{\bar{r}} - \frac{df}{d\bar{r}}\right)\frac{d\bar{D}_{r\theta}}{d\bar{r}} \\
&+ \frac{1}{\bar{r}}\left(-\frac{k^2 f}{\bar{r}} + \frac{df}{d\bar{r}}\right)\frac{d^2 \bar{D}_{r\theta}}{d\bar{r}^2} + \frac{4k^2}{\bar{r}^2}\left(-\frac{f}{\bar{r}^2} + \frac{1}{\bar{r}}\frac{df}{d\bar{r}} - \frac{d^2 f}{d\bar{r}^2}\right)\bar{D}_{ss} \\
&+ \frac{4k^2}{\bar{r}^2}\left(\frac{f}{\bar{r}} - \frac{df}{d\bar{r}}\right)\frac{d\bar{D}_{ss}}{d\bar{r}} - \frac{12}{\bar{H}^2\lambda_r\lambda_\theta}\left[\bar{\sigma}_{rr}\frac{d^2 f}{d\bar{r}^2} + \frac{\bar{\sigma}_{\theta\theta}}{\bar{r}}\left(\frac{df}{d\bar{r}} - \frac{k^2 f}{\bar{r}}\right)\right] = 0
\end{aligned} \tag{37}$$

The corresponding homogeneous boundary conditions are

$$f|_{\bar{r}=\frac{A}{B}} = 0 \tag{38a}$$

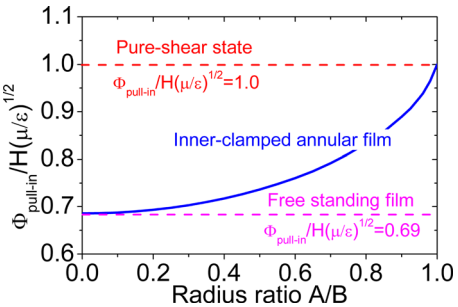

Fig. 4 Dependence of the critical voltage of inducing pull-in instability of the annular DE film on the ratio between its inner radius and outer radius. When the ratio between inner radius and outer radius approaches zero, the annular film becomes a free-standing film; when the ratio approaches one, the deformation state of the film is pure-shear.

$$\left.\frac{df}{d\bar{r}}\right|_{\bar{r}=\frac{A}{B}}=0 \tag{38b}$$

$$\left[\bar{D}_{rr}\frac{d^2f}{d\bar{r}^2}+\bar{D}_{r\theta}\left(\frac{1}{\bar{r}}\frac{df}{d\bar{r}}-\frac{k^2}{\bar{r}^2}f\right)\right]\Bigg|_{\bar{r}=\frac{b}{B}}=0 \tag{38c}$$

$$\left[\left(\frac{1}{\bar{r}}\frac{d^2f}{d\bar{r}^2}+\frac{d^3f}{d\bar{r}^3}\right)\bar{D}_{rr}+\frac{1}{\bar{r}^2}\left(\frac{f}{\bar{r}}-\frac{df}{d\bar{r}}\right)\bar{D}_{\theta\theta}+\frac{k^2}{\bar{r}^2}\left(\frac{f}{\bar{r}}-\frac{df}{d\bar{r}}\right)\bar{D}_{r\theta}+\frac{4k^2}{\bar{r}^2}\left(\frac{f}{\bar{r}}-\frac{df}{d\bar{r}}\right)\bar{D}_{ss}+\left(-\frac{k^2f}{\bar{r}^2}+\frac{f}{\bar{r}}\frac{df}{d\bar{r}}\right)\frac{d\bar{D}_{r\theta}}{d\bar{r}}+\frac{d^2f}{d\bar{r}^2}\frac{d\bar{D}_{rr}}{d\bar{r}}\right]\Bigg|_{\bar{r}=\frac{b}{B}}=0 \tag{38d}$$

In Eqs. (37) and (38), we define the following dimensionless quantities: dimensionless thickness: $\bar{H}=H/B$; dimensionless membrane stresses: $\bar{\sigma}_{rr}=\sigma_{rr}/\mu$ and $\bar{\sigma}_{\theta\theta}=\sigma_{\theta\theta}/\mu$; dimensionless bending/twisting stiffness: $\bar{D}_{rr}=2(\lambda_r^{-5}\lambda_\theta^{-5}+\lambda_r^{-1}\lambda_\theta^{-3})$, $\bar{D}_{\theta\theta}=2(\lambda_r^{-5}\lambda_\theta^{-5}+\lambda_r^{-3}\lambda_\theta^{-1})$, $\bar{D}_{r\theta}=2\lambda_r^{-5}\lambda_\theta^{-5}$, and $\bar{D}_{ss}=(\lambda_r^{-1}\lambda_\theta^{-3}+\lambda_r^{-3}\lambda_\theta^{-1})/2$. In the equations above, dimensionless thickness $\bar{H}$ and the ratio between inner radius and outer radius of the annular DE film A/B are the only two system parameters which can be varied in experiments. The membrane stresses in the radial and hoop directions: $\bar{\sigma}_{rr}$ and $\bar{\sigma}_{\theta\theta}$, and the bending/twisting stiffness both depend on the electrical field E or voltage Φ, which can be regarded as loading parameters for the system. For a given set of parameters: $\bar{H}$ and A/B, we can solve the eigenvalue problem in Eq. (37) with boundary conditions (38) numerically by using the function *bvp4c* in MATLAB. The characteristic equation determines the critical condition, namely, voltage, for the onset of wrinkles, and the associated eigenvectors give the mode of wrinkling.

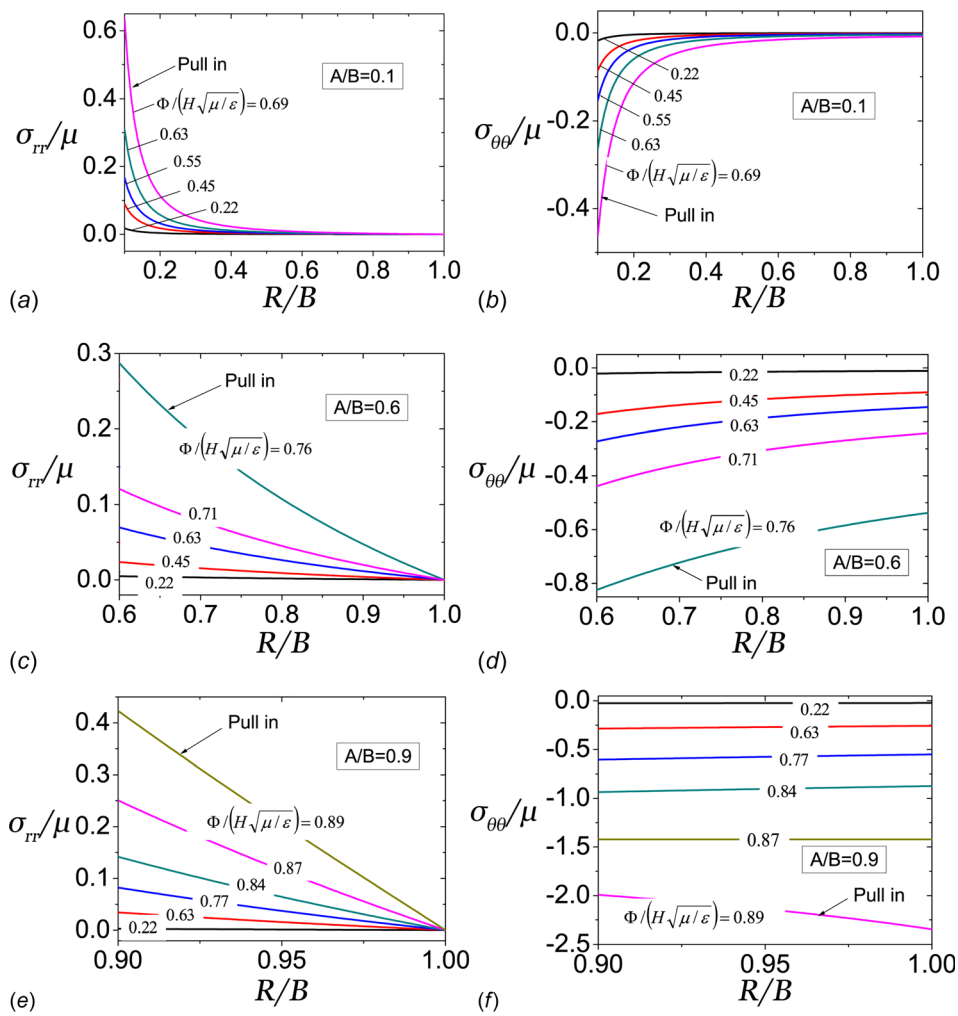

Fig. 5 Distributions of radial stress and hoop stress in the DE film without wrinkles, for several voltages and radius ratios: (*a*) and (*b*) *A*/*B* = 0.1, (*c*) and (*d*) *A*/*B* = 0.6, and (*e*) and (*f*) *A*/*B* = 0.9. The radial stress in the film is tensile, while the hoop stress is compressive. The compressive hoop stress may wrinkle the DE film.

4 Results and Discussion

Using the shooting method, we solve the ODEs of Eqs. (7) and (8) associated with the boundary conditions (9) and (10) for a constrained annular DE film without wrinkle formation. Figure 3 plots the distributions of radial stretch and hoop stretch in the annular DE film, for several different voltages and ratios between inner and outer radius of the film. With increasing the voltage, both radial stretch and hoop stretch increase.

As shown in Fig. 3, when the voltage is larger than a critical value, no equilibrium solution can be found, which corresponds to pull-in instability of the DE film. Pull-in instability is one of the most important electromechanical failure modes in DE structures [19–21]. The critical voltage for the pull-in instability increases with the increase in the ratio A/B as plotted in Fig. 4. When the ratio A/B approaches zero, the annular DE film behaves like a free-standing film. It has been shown in previous studies that the critical voltage for the pull-in instability of a free-standing neo-Hookean DE film is $\Phi_{\text{pull-in}}/(H\sqrt{\mu/\varepsilon}) = 0.69$ [19]. When the ratio A/B approaches one, the deformation state in the annular DE film is close to pure-shear. It can also be easily shown that for a DE film with voltage-induced pure-shear deformation, the normalized voltage for pull-in instability is $\Phi_{\text{pull-in}}/(H\sqrt{\mu/\varepsilon}) = 1$. Both two limiting scenarios discussed earlier have been plotted in Fig. 4.

Figure 5 plots the distribution of radial stress and hoop stress in the annular DE film without wrinkle formation for several different radius ratios and applied voltages. The results show that the radial stress in the DE film is tensile, while the hoop stress in the film is compressive. For a given radius ratio, both radial stress and hoop stress in the DE film increase with increasing the voltage. In addition, the radial stress in the DE film monotonically decreases from the inner boundary to the outer boundary as shown in Figs. 5(*a*), 5(*c*), and 5(*e*). The distribution of the hoop stress is little bit more intricate. For small radius ratio, the hoop stress in the DE film monotonically increases from the inner boundary to outer boundary. However, for big radius ratio, the hoop stress in the DE film may monotonically decrease from the inner boundary to the outer boundary when the voltage is large as shown in Fig. 5(*f*).

When the voltage is high enough, compressive hoop stress can induce wrinkles in the annular DE film as shown in our experiments (Fig. 1). By solving the eigenvalue problem formulated in Sec. 3, we can calculate the critical voltage for the onset of wrinkles with different wavelengths in the DE film for different values of A/B. Our calculation results are plotted in Fig. 6. For a given value of A/B and wavenumber k of wrinkles, the voltage for the onset of wrinkles decreases with decreasing the thickness of the film, namely, H/B. The results suggest that lower voltage is needed to trigger wrinkle formation in thinner DE films. For different values of A/B, the wrinkling mode which needs the lowest critical voltage is also different. For instance, in Fig. 6(*a*), for $A/B = 0.1$, the wrinkling mode with $k = 2$ needs the lowest voltage; in Fig. 6(*b*), for $A/B = 0.3$, the critical mode is $k = 3$. Figures 6(*c*) and 6(*d*) show that the critical modes are $k = 4$ and $k = 6$ or 7 for $A/B = 0.5$ and 0.7, respectively. In Figs. 6(*a*)–6(*d*), we also plot the voltage for inducing pull-in instability in the DE film. For a thick DE film, the critical voltage for wrinkling may be even larger than the critical voltage for pull-in instability. Therefore, for thick DE films, the wrinkles form after pull-in instability, which can be consequently regarded as an indication of material failure.

In Fig. 7, we plot the dependence of critical wrinkling mode on the ratio between the inner radius and outer radius of the DE film for two different film thicknesses: $H/B = 0.02$ and 0.005, respectively. The result shows that the wavenumber of the critical wrinkling mode increases with increasing the value of A/B. The trend agrees well with the wrinkling instability observed in a constrained annular film induced by differential swelling or plastic deformation [48,50]. The results also show that for a given radius ratio, the DE film with different thickness may also have different critical wrinkling modes. For the ratio: $A/B = 0.75$, the critical wrinkling mode of the DE film with thickness $H/B = 0.02$ is $k = 7$,

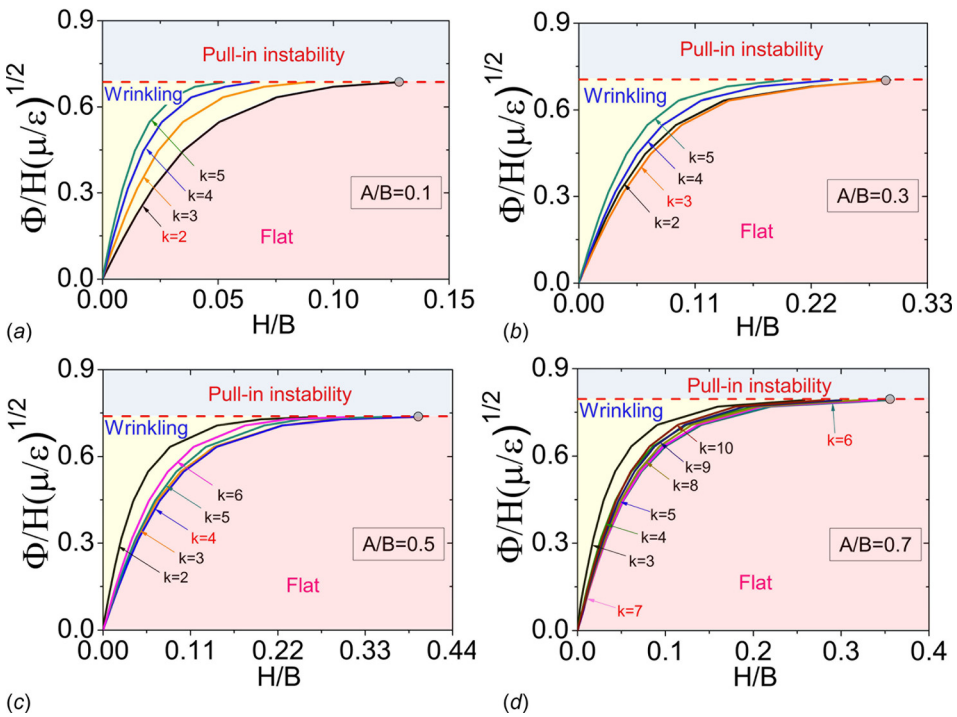

Fig. 6 Dependence of critical voltage for inducing wrinkling instability on the thickness of the DE film, for several radius ratios and wrinkling modes: (*a*) $A/B = 0.1$, (*b*) $A/B = 0.3$, (*c*) $A/B = 0.5$, and (*d*) $A/B = 0.7$. For larger film thickness, the voltage for inducing pull-in instability is smaller than the voltage for inducing wrinkling in the film.

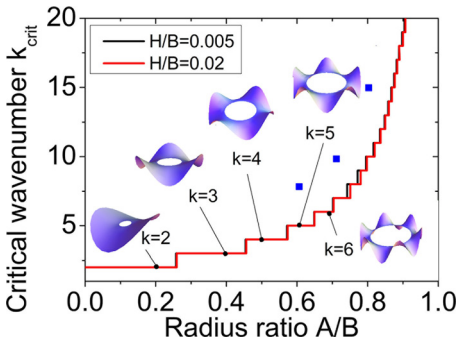

Fig. 7 Dependence of the wavenumber of the critical wrinkling mode on the radius ratio for two different film thicknesses *H/B* = 0.02 and 0.005. The three dots are experimental results from Fig. 1.

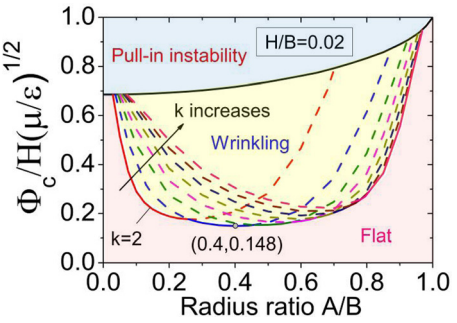

Fig. 8 A phase diagram of a constrained annular DE film with thickness *H/B* = 0.02. Depending on the ratio between the inner radius and outer radius of the film and the magnitude of applied voltage, the film may stay in a flat and stable phase, wrinkling phase, or pull-in instability phase. The boundary between the flat phase and wrinkling phase of the DE film is given by the dependence of critical voltage for wrinkling on its radius ratio *A/B*. For the annular DE film with the radius ratio: *A/B* = 0.4, the required voltage to induce wrinkles in the film is the lowest.

while $k = 8$ for the film with $H/B = 0.005$. However, it is noted that when A/B is close to one, thin plate theory adopted in this article will not be valid anymore.

In the experiment, it is usually challenging to precisely measure the critical voltage for the onset of wrinkles in a DE film. However, the wavenumber of wrinkles in the DE film can be easily measured as shown in Fig. 1. The experimental results of the wavenumber of wrinkles in annular DE films for three different values of A/B are plotted together with our predictions as shown in Fig. 7. The wavenumber of wrinkles in the experiments is consistently larger than the predictions. This difference can be understood as follows: as described in Sec. 2 and also shown in Fig. 1, to avoid electrical arcing, a gap near the free edge of the annular DE film is intentionally not coated with electrode. Due to the additional constraint from the gap which is not considered in our model, stretching free energy penalty (compared to bending energy penalty) in the film is actually larger than the prediction. Therefore, in the experiments, wavenumber of wrinkles in the film is larger than predictions to reduce stretching energy penalty.

Based on our calculation, we construct a phase diagram for a constrained DE annular film with the thickness $H/B = 0.02$ as shown in Fig. 8. Depending on the radius ratio and magnitude of voltage, the DE film may stay in one of the three phases: flat, wrinkling, and pull-in instability. It can be seen from Fig. 8 that the critical voltage for triggering wrinkling in the DE film first decreases and then increases with increasing the ratio between inner radius and outer radius. When $A/B = 0.4$, the required voltage to induce wrinkles in the film is the lowest.

5 Conclusions

In this paper, we formulate a linear plate theory for a DE film under electromechanical loading with small three-dimensional deformation field superposed onto a finite two-dimensional deformation. Based on the theory, we investigate the formation and morphology of wrinkles in an annular DE film subjected to a voltage and clamped on its inner radius. The theoretical predictions of wrinkling in the DE film agree well with our experimental observations. Furthermore, we show that for certain ranges of ratio between inner radius and outer radius of the DE film, the critical voltage of inducing pull-in instability of the system can be lower than the critical voltage of inducing wrinkles in the film. As a result, we construct a phase diagram with three different regions depending on the magnitude of voltage and the ratio between inner radius and outer radius of an annular DE film: (1) the region corresponding to stable and flat configuration of the film; (2) wrinkling region; and (3) the region for pull-in instability. The results obtained in this paper and the methodology developed here will be useful for the future design of DE structures.

Funding Data

- Anhui Provincial Universities Natural Science Research Project (Grant Nos. KJ2015A046 and KJ2016A147).
- National Natural Science Foundation of China (Grant Nos. 11402001, 11472005, and 51408005).
- National Science Foundation (Grant No. CMMI-1538137).

References

[1] Carpi, F., De Rossi, D., Kornbluh, R., Pelrine, R., and Sommer-Larsen, P., 2008, *Dielectric Elastomers as Electromechanical Transducers*, Elsevier, Oxford, UK.

[2] O'Halloran, A., O'Malley, F., and McHugh, P., 2008, "A Review on Dielectric Elastomer Actuators, Technology, Applications, and Challenges," J. Appl. Phys., **104**(7), p. 071101.

[3] Kornbluh, R. D., Pelrine, R., Prahlad, H., Wong-Foy, A., McCoy, B., Kim, S., Eckerle, J., and Low, T., 2012, "Dielectric Elastomers: Stretching the Capabilities of Energy Harvesting," MRS Bull., **37**(3), pp. 246–253.

[4] Kornbluh, R. D., Pelrine, R., Prahlad, H., Wong-Foy, A., McCoy, B., Kim, S., Eckerle, J., and Low, T., 2012, "From Boots to Buoys: Promises and Challenges of Dielectric Elastomer Energy Harvesting," *Electroactivity in Polymeric Materials*, Springer, New York.

[5] Brochu, P., and Pei, Q. B., 2010, "Advances in Dielectric Elastomers for Actuators and Artificial Muscles," Macromol. Rapid Commun., **31**(1), pp. 10–36.

[6] Shian, S., Bertoldi, K., and Clarke, D. R., 2015, "Dielectric Elastomer Based "Grippers" for Soft Robotics," Adv. Mater., **27**(43), pp. 6814–6819.

[7] Wang, Q., Gossweiler, G. R., Craig, S. L., and Zhao, X. H., 2014, "Cephalopod-Inspired Design of Electro-Mechano-Chemically Responsive Elastomers for On-Demand Fluorescent Patterning," Nat. Commun., **5**, p. 4899.

[8] Shivapooja, P., Wang, Q., Orihuela, B., Rittschof, D., López, G. P., and Zhao, X. H., 2013, "Bioinspired Surfaces With Dynamic Topography for Active Control of Biofouling," Adv. Mater., **25**(10), pp. 1430–1434.

[9] Keplinger, C., Sun, J. Y., Foo, C. C., Rothemund, P., Whitesides, G. M., and Suo, Z. G., 2013, "Stretchable, Transparent, Ionic Conductors," Science, **341**(6149), pp. 984–987.

[10] Anderson, I. A., Hale, T., Gisby, T., Inamura, T., McKay, T., O'Brien, B., Walbran, S., and Calius, E. P., 2010, "A Thin Membrane Artificial Muscle Rotary Motor," Appl. Phys. A, **98**(1), pp. 75–83.

[11] Xu, D., Tairych, A., and Anderson, I. A., 2015, "Localised Strain Sensing of Dielectric Elastomers in a Stretchable Soft-Touch Musical Keyboard," Proc. SPIE, **9430**, p. 943025.

[12] Dorfmann, A., and Ogden, R. W., 2005, "Nonlinear Electroelasticity," Acta Mech., **174**(3–4), pp. 167–183.

[13] Goulbourne, N. C., Mockensturm, E. M., and Frecker, M. I., 2005, "A Nonlinear Model for Dielectric Elastomer Membranes," ASME J. Appl. Mech., **72**(6), pp. 899–906.

[14] McMeeking, R. M., and Landis, C. M., 2005, "Electrostatic Forces and Stored Energy for Deformable Dielectric Materials," ASME J. Appl. Mech., **72**(4), pp. 581–590.

[15] Vu, D. K., Steinmann, P., and Possart, G., 2007, "Numerical Modelling of Non-Linear Electroelasticity," Int. J. Numer. Methods Eng., **70**(6), pp. 685–704.

[16] Suo, Z. G., Zhao, X. H., and Greene, W. H., 2008, "A Nonlinear Field Theory of Deformable Dielectrics," J. Mech. Phys. Solids, **56**(2), pp. 467–486.

[17] O'Brien, B., McKay, T., Calius, E., Xie, S., and Anderson, I., 2009, "Finite Element Modelling of Dielectric Elastomer Minimum Energy Structures," Appl. Phys. A, **94**(3), pp. 507–514.

[18] Trimarco, C., 2009, "On the Dynamics of Electromagnetic Bodies," Int. J. Adv. Eng. Sci. Appl. Math., **1**(4), pp. 157–162.
[19] Zhao, X. H., and Suo, Z. G., 2007, "Method to Analyze Electromechanical Stability of Dielectric Elastomers," Appl. Phys. Lett., **91**(6), p. 061921.
[20] Norris, A. N., 2008, "Comment on 'Method to Analyze Electromechanical Instability of Dielectric Elastomers'," Appl. Phys. Lett., **92**(2), p. 026101.
[21] Zhou, J. X., Hong, W., Zhao, X. H., Zhang, Z. Q., and Suo, Z. G., 2008, "Propagation of Instability in Dielectric Elastomers," Int. J. Solids Struct., **45**(13), pp. 3739–3750.
[22] Wang, Q., Tahir, M., Zhang, L., and Zhao, X. H., 2011, "Electro-Creasing Instability in Deformed Polymers: Experiment and Theory," Soft Matter, **7**(14), pp. 6583–6589.
[23] Li, T. F., Keplinger, C., Baumgartner, R., Bauer, S., Yang, W., and Suo, Z. G., 2013, "Giant Voltage-Induced Deformation in Dielectric Elastomers Near the Verge of Snap-Through Instability," J. Mech. Phys. Solids, **61**(2), pp. 611–628.
[24] Liang, X. D., and Cai, S. Q., 2015, "Shape Bifurcation of a Spherical Dielectric Elastomer Balloon Under the Actions of Internal Pressure and Electric Voltage," ASME J. Appl. Mech., **82**(10), p. 101002.
[25] Bertoldi, K., and Gei, M., 2011, "Instabilities in Multilayered Soft Dielectrics," J. Mech. Phys. Solids, **59**(1), pp. 18–42.
[26] Dorfmann, L., and Ogden, R. W., 2014, "Instabilities of an Electroelastic Plate," Int. J. Eng. Sci., **77**, pp. 79–101.
[27] Plante, J. S., and Dubowsky, S., 2006, "Large-Scale Failure Modes of Dielectric Elastomer Actuators," Int. J. Solids Struct., **43**(25), pp. 7727–7751.
[28] De Tommasi, D., Puglisi, G., and Zurlo, G., 2011, "Compression-Induced Failure of Electroactive Polymeric Thin Films," Appl. Phys. Lett., **98**(12), p. 123507.
[29] De Tommasi, D., Puglisi, G., and Zurlo, G., 2013, "Electromechanical Instability and Oscillating Deformations in Electroactive Polymer Films," Appl. Phys. Lett., **102**(1), p. 011903.
[30] De Tommasi, D., Puglisi, G., and Zurlo, G., 2013, "Inhomogeneous Deformations and Pull-In Instability in Electroactive Polymeric Films," Int. J. Nonlinear Mech., **57**, pp. 123–129.
[31] Zurlo, G., 2013, "Non-Local Elastic Effects in Electroactive Polymers," Int. J. Nonlinear Mech., **56**, pp. 115–122.
[32] De Tommasi, D., Puglisi, G., and Zurlo, G., 2014, "Failure Modes in Electroactive Polymer Thin Films With Elastic Electrodes," J. Phys. D, **47**(6), p. 065502.
[33] Kollosche, M., Kofod, G., Suo, Z. G., and Zhu, J., 2015, "Temporal Evolution and Instability in a Viscoelastic Dielectric Elastomer," J. Mech. Phys. Solids, **76**, pp. 47–64.
[34] Lu, T., An, L., Li, J., Yuan, C., and Wang, T. J., 2015, "Electro-Mechanical Coupling Bifurcation and Bulging Propagation in a Cylindrical Dielectric Elastomer Tube," J. Mech. Phys. Solids, **85**, pp. 160–175.
[35] Mao, G., Huang, X., Diab, M., Li, T., Qu, S., and Yang, W., 2015, "Nucleation and Propagation of Voltage-Driven Wrinkles in an Inflated Dielectric Elastomer Balloon," Soft Matter, **11**(33), pp. 6569–6575.
[36] Mao, G., Huang, X., Diab, M., Liu, J., and Qu, S., 2016, "Controlling Wrinkles on the Surface of a Dielectric Elastomer Balloon," Extreme Mech. Lett., **9**(Pt. 1), pp. 139–146.
[37] Liu, X., Li, B., Chen, H., Jia, S., and Zhou, J., 2016, "Voltage-Induced Wrinkling Behavior of Dielectric Elastomer," J. Appl. Polym. Sci., **133**(14), p. 43258.
[38] Mao, G., Wu, L., Liang, X., and Qu, S., 2017, "Morphology of Voltage-Triggered Ordered Wrinkles of a Dielectric Elastomer Sheet," ASME J. Appl. Mech., **84**(11), p. 111005.
[39] Huang, R., and Suo, Z. G., 2012, "Electromechanical Phase Transition in Dielectric Elastomers," Proc. R. Soc. A, **468**(2140), pp. 1014–1040.
[40] Park, H. S., Suo, Z. G., Zhou, J., and Klein, P. A., 2012, "A Dynamic Finite Element Method for Inhomogeneous Deformation and Electromechanical Instability of Dielectric Elastomer Transducers," Int. J. Solids Struct., **49**(15), pp. 2187–2194.
[41] Zhu, J., Kollosche, M., Lu, T., Kofod, G., and Suo, Z. G., 2012, "Two Types of Transitions to Wrinkles in Dielectric Elastomers," Soft Matter, **8**(34), pp. 8840–8846.
[42] Díaz-Calleja, R., Llovera-Segovia, P., Dominguez, J. J., Rosique, M. C., and Lopez, A. Q., 2013, "Theoretical Modelling and Experimental Results of Electromechanical Actuation of an Elastomer," J. Phys. D, **46**(23), p. 235305.
[43] Diaz-Calleja, R., Llovera-Segovia, P., and Quijano-López, A., 2014, "Bifurcations in Biaxially Stretched Highly Non-Linear Materials Under Normal Electric Fields," Europhys. Lett., **108**(2), p. 26002.
[44] Godaba, H., Zhang, Z. Q., Gupta, U., Foo, C. C., and Zhu, J., 2017, "Dynamic Pattern of Wrinkles in a Dielectric Elastomer," Soft Matter, **13**(16), pp. 2942–2951.
[45] Conn, A. T., and Rossiter, J., 2012, "Harnessing Electromechanical Membrane Wrinkling for Actuation," Appl. Phys. Lett., **101**(17), p. 171906.
[46] Xie, Y. X., Liu, J. C., and Fu, Y. B., 2016, "Bifurcation of a Dielectric Elastomer Balloon Under Pressurized Inflation and Electric Actuation," Int. J. Solids Struct., **78–79**, pp. 182–188.
[47] Piñeirua, M., Tanaka, N., Roman, B., and Bico, J., 2013, "Capillary Buckling of a Floating Annulus," Soft Matter, **9**(46), pp. 10985–10992.
[48] Mora, T., and Boudaoud, A., 2006, "Buckling of Swelling Gels," Eur. Phys. J. E, **20**(2), pp. 119–124.
[49] Dervaux, J., and Amar, M. B., 2008, "Morphogenesis of Growing Soft Tissues," Phys. Rev. Lett., **101**(6), p. 068101.
[50] Coman, C. D., and Bassom, A. P., 2007, "On the Wrinkling of a Pre-Stressed Annular Thin Film in Tension," J. Mech. Phys. Solids, **55**(8), pp. 1601–1617.
[51] Davidovitch, B., Schroll, R. D., Vella, D., Adda-Bedia, M., and Cerda, E. A., 2011, "Prototypical Model for Tensional Wrinkling in Thin Sheets," Proc. Natl. Acad. Sci. U.S.A., **108**(45), pp. 18227–18232.
[52] Ventsel, E., and Krauthammer, T., 2001, *Thin Plates and Shells: Theory, Analysis, and Applications*, Marcel Dekker, New York.